

Nanoscale

Accepted Manuscript



This is an *Accepted Manuscript*, which has been through the Royal Society of Chemistry peer review process and has been accepted for publication.

Accepted Manuscripts are published online shortly after acceptance, before technical editing, formatting and proof reading. Using this free service, authors can make their results available to the community, in citable form, before we publish the edited article. We will replace this *Accepted Manuscript* with the edited and formatted *Advance Article* as soon as it is available.

You can find more information about *Accepted Manuscripts* in the [Information for Authors](#).

Please note that technical editing may introduce minor changes to the text and/or graphics, which may alter content. The journal's standard [Terms & Conditions](#) and the [Ethical guidelines](#) still apply. In no event shall the Royal Society of Chemistry be held responsible for any errors or omissions in this *Accepted Manuscript* or any consequences arising from the use of any information it contains.

PAPER

Competitive adsorption of binary CO₂/CH₄ mixture in nanoporous carbons: Effect of edge-functionalization

Cite this: DOI: 10.1039/x0xx00000x

Xiaoqing Lu,^{a*} Dongliang Jin,^a Shuxian Wei,^a Mingmin Zhang,^a Qing Zhu,^a Xiaofan Shi,^a Zhigang Deng,^a Wenyue Guo,^{a*} and Wenzhong Shen^b

Received XXth XXXXXX XXXX,
Accepted 00th XXXXXX XXXX

DOI: 10.1039/x0xx00000x

www.rsc.org/Nanoscale

The effect of edge-functionalization has been investigated, for the first time, on the competitive adsorption of binary CO₂/CH₄ mixture in nanoporous carbons (NPCs) by combining density functional theory (DFT) and grand canonical Monte Carlo (GCMC) simulation. Our results show that edge-functionalization has a more positive effect on the single-component adsorption of CO₂ than CH₄, and therefore significantly enhancing the selectivity of CO₂ over CH₄, in the sequence of NH₂-NPC > COOH-NPC > OH-NPC > H-NPC > NPC at low pressure. The enhanced adsorption originates essentially from the effects of (1) the conducive environment with large pore size and effective accessible surface area, (2) the high electronegativity/electropositivity, (3) the strong adsorption energy, and (4) the large electrostatic contribution, due to the inductive effect/direct interaction of the embedded edge-functionalized groups. The larger difference from these effects results in the higher competitive adsorption advantage of CO₂ in binary CO₂/CH₄ mixture. Temperature has a negative effect on the gas adsorption, but no obvious influence on the electrostatic contribution on selectivity. With the increase of pressure, the selectivity of CO₂ over CH₄ first decreases sharply and subsequently flattens out to a constant value. This work highlights the potential of edge-functionalized NPCs in competitive adsorption, capture, and separation for binary CO₂/CH₄ mixture, and provides an effective and superior alternative strategy in the design and screening of adsorbent materials for carbon capture and storage.

1. Introduction

Carbon capture and storage (CCS), as a promising approach to mitigate the greenhouse gas emission, has attracted considerable attention during the past several years.¹ Adsorbent materials with high CO₂ adsorption capacity and excellent selectivity of CO₂ over other gases are essential for CCS. Through materials, such as natural geological coalbeds and organic components of gas-shale, CO₂-injection can effectively replace or displace CH₄ to enhance CH₄ recovery and CO₂ storage as a best-of-both-worlds solution.²⁻⁴ Experimentally, a wide diversity of adsorbent materials, such as graphite/graphene, carbon nanotubes (CNTs), porous organic polymers (POPs), covalent organic frameworks (COFs), and metal

organic frameworks (MOFs) have been designed and synthesized for potential use in CCS process.^{5,6} Among these materials, nanoporous carbons (NPCs) have been proven to be competitive candidates by virtue of their effective surface modification and functionalization,⁷⁻¹¹ due to their high specific surface area, moderate heat of adsorption, low-cost preparation, relatively easy regeneration, and less sensitivity to humidity effect than the other CO₂-philic materials.

Research on the adsorption behavior of single-component CO₂/CH₄ and their binary mixture in NPCs is conducted continuously.¹²⁻²² Jain *et al.*¹⁵⁻¹⁷ developed a new molecular modeling on NPCs by using the reverse Monte Carlo (RMC) method, and found that the calculated adsorption amount and isosteric heat were in good agreement with the experimental results. Brochard *et al.*¹⁸ studied the competitive adsorption of binary CO₂/CH₄ mixture in NPCs, and described the desorption behavior of CH₄ with the CO₂-injection in detail. Tenney *et al.*¹⁹ performed structurally and chemically heterogeneous modification on graphite surface, and observed that CO₂ adsorption generally increased with the increase of surface oxygen content because of the enhanced adsorbate-adsorbent interactions. We²⁰ investigated the effect of surface-functionalization on CH₄ adsorption in graphitic pores, and

^a College of Science, China University of Petroleum, Qingdao, Shandong 266580, P. R. China

^b Department of Physics, Shanghai Jiao Tong University, Shanghai 200240, P. R. China

E-mail address: luxq@upc.edu.cn and wyguo@upc.edu.cn; Tel: +86 532 8698 3372; Fax: +86 532 8698 3363

†Electronic Supplementary Information (ESI) available: Optimized CO₂/CH₄ structures. Validation of computational methodology. Computational method of pore volume. Atomic partial charge. Stable adsorption configurations of CO₂/CH₄ on coronene. Absolute adsorption isotherms of CO₂/CH₄ in their mixture. See DOI:10.1039/b000000x/

found that the effect from electrostatic interaction of a gas framework decreased the adsorption capacity in the sequence of perfect > carbonyl > carbonyl–hydroxyl > hydroxyl–hydroxyl > hydroxyl > carboxyl > epoxy at a pressure range of 0.0–0.2 MPa. Wilcox *et al.*^{1,21,22} indicated that the introduction of O-containing functional groups on graphite surface could enhance the adsorption capacity of CO₂ and the selectivity of CO₂ over CH₄ and N₂. More interestingly, the embedded position of functional groups has a significant effect on their gas adsorption behaviors. Kandagal *et al.*²³ reported that functional groups embedded on the edge of graphene nanoribbons would be preferable sites for CH₄ adsorption. Furthermore, competitive adsorption behavior of gas mixture is dependent on the surrounding or operational conditions, such as temperature and pressure. Kurniawan *et al.*⁸ explored the competitive adsorption of binary CO₂/CH₄ mixture in an idealized slit pore, and found that with the increase of pressure, the selectivity of CO₂ over CH₄ initially increased to a maximum value and then decreased to a constant value. However, investigation on the effects of edge-functionalization on the adsorption capacity and selectivity of CO₂ over CH₄ in NPCs is still scarce, not to mention studies under complicated surrounding conditions.

The present work investigates the effect of edge-functionalization on the competitive adsorption of binary CO₂/CH₄ mixture in NPCs at a wide range of pressure and temperature. DFT calculations are performed to optimize the geometries of CO₂/CH₄ and edge-functionalized basic units. GCMC simulations are carried out to predict the thermodynamic equilibrium properties of single-component CO₂/CH₄ and their binary mixture in edge-functionalized NPCs. The intrinsic enhancement mechanisms of the adsorption capacity and selectivity of CO₂ over CH₄ are elucidated, including the effect of edge-functionalization on (1) pore topology and morphology, (2) atomic partial charge, (3) adsorption energy, and (4) electrostatic interaction of gas-framework. This theoretical approach elucidates the intrinsic enhancement mechanism, and highlights the potential use of edge-functionalized NPCs in the competitive adsorption, capture, and separation of binary CO₂/CH₄ mixture, and therefore offering an effective and superior alternative approach in the design and screening of adsorbent materials for CCS application.

2. Model and Computing Methodology

2.1 Density Functional Theory (DFT)

Four functional groups were considered to improve gas adsorption capacity and selectivity performance of NPCs, *i.e.*, hydrogen (H–), hydroxyl (OH–), amine (NH₂–) and carboxyl (COOH–). As shown in Fig. 1, a coronene-shaped graphitic basis unit was chosen as the electron structure model for quantum-chemistry calculation. Mulliken charge analysis was performed to calculate the atomic partial charge, as basic input parameters in molecular simulation to describe the electrostatic interaction. The B3LYP functional in conjunction with the 6-31+g (d, p) basis set in Gaussian 09

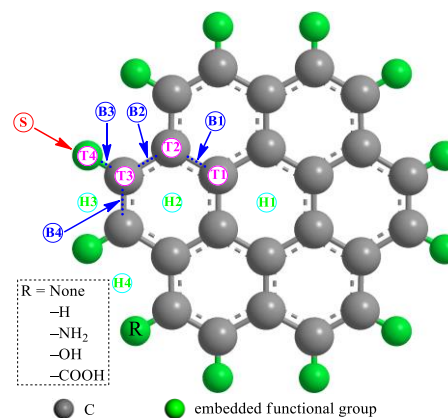


Fig. 1 Initial configurations of CO₂/CH₄ adsorption on edge-functionalized basis unit. Nomenclature: H, position above the center of a benzene ring in basis unit; T, position at the top of C atom or the atom connected to the functional group; B, position above the bond center; and S, side position in the plane of the functional group.

package²⁴ was adopted due to the good balance of accuracy and efficiency on the atomic charge analysis.^{25–27}

Single gas molecule adsorbed on the basis unit was arranged as the gas-framework interaction model to investigate the relative reactivity. Fig. 1 illustrates the possible adsorption sites, *i.e.*, one side (S), four bridge (B), four top (T) and four hcp (H) configurations (marked as 1, 2, 3 and 4, respectively). A single C–H bond of CH₄ directly toward the basis unit was chosen as the initial configuration based on previous *ab initio* studies;²⁸ and linear CO₂ was perpendicular and parallel to basal plane for S and other sites, respectively. The minimum energy configurations of single CO₂/CH₄ molecule adsorbed on edge-functionalized basis units were calculated by Dmol³ program package.^{29,30} Generalized gradient approximation (GGA) with the Perdew–Burke–Ernzerhof (PBE)³¹ functional, which was widely adopted to describe the gas-graphene interaction due to the high accuracy in the description of long-range distance force like van der Waals potential, was used for describing the exchange–correlation interaction.^{32,33} The density functional semicore pseudopotential (DSPP)³⁴ method in conjunction with the localized double-numerical basis with polarization (DNP) functional was chosen for all the atoms.

2.2 Force fields

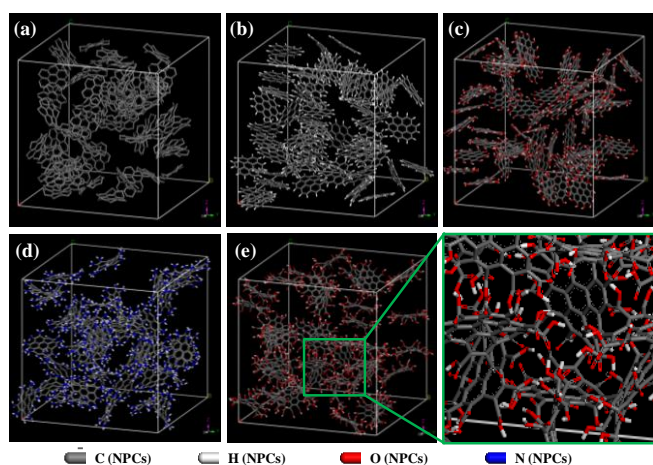
CH₄ was modeled as a rigid regular tetrahedron molecule with five charged Lennard–Jones (LJ) interaction sites, and CO₂ was modeled as a rigid linear molecule with three charged LJ interaction sites. The 5-site CH₄ model is more accurate to describe the adsorbate–adsorbent interaction than the 1-site model since the latter misses the atomic partial charge information. For CO₂ and CH₄, the LJ potential parameters were taken from the TraPPE model, which were developed by Potoff, Siepmann³⁵ and Sun³⁶; and atomic partial charge and geometrical configure were taken from our *ab initio* results, as shown in Fig. S1 (see ESI†). For NPCs framework, the atomic LJ potential parameters were taken from the universal force

Table 1 Lennard-Jones parameters and atomic partial charges for CH₄, CO₂, and NPCs

Atom	Gas molecule models				UFF force field				
	C(CH ₄)	H(CH ₄)	C(CO ₂)	O(CO ₂)	C	H	O	N	He
σ (Å)	3.40	2.65	2.80	3.05	3.40	2.57	3.12	3.26	2.64
ε (K)	55.05	7.90	27.00	79.00	29.13	22.12	34.72	34.75	10.90
q (e)	-0.612	0.153	0.748	-0.374	--	--	--	--	0.000

Table 2 Atomic partial charges by Mulliken charge analysis

Functional group	C of basis unit			Functional group			
	direct-connected	peripheral	others	C	O	H	N
None	-0.096 ~ -0.095	0.223 ~ 0.224	-0.033 ~ -0.030	--	--	--	--
H-	-0.244 ~ -0.243	0.435 ~ 0.436	-0.206 ~ -0.202	--	--	0.127	--
OH-	-0.228 ~ 0.175	0.650 ~ 0.967	-0.490 ~ -0.449	--	-0.739 ~ -0.548	0.404 ~ 0.456	--
NH ₂ -	-0.790 ~ -0.094	0.530 ~ 1.160	0.010 ~ 0.113	--	--	0.267 ~ 0.367	-0.879 ~ -0.577
COOH-	-0.410 ~ 0.796	0.109 ~ 0.490	-0.298 ~ 0.246	-0.407 ~ 0.743	-0.455 ~ -0.251	0.370 ~ 0.404	--

**Fig. 2** Visualization of unit cell of edge-functionalized NPCs: (a) NPC; (b) H-NPC; (c) OH-NPC; (d) NH₂-NPC; (e) COOH-NPC.

field (UFF)³⁷, which was proven to use successfully in metal complexes³⁸, organic molecules³⁹, and main group⁴⁰, *etc.* The LJ potential parameters and atomic partial charges used were provided in Table 1, and the atomic partial charges of NPCs framework were provided in Table 2. All the interaction parameters conform to Lorentz-Berthelot mixing rules, *i.e.*, $\varepsilon_{ij} = (\varepsilon_{ii} \varepsilon_{jj})^{1/2}$, $\sigma_{ij} = (\sigma_{ii} + \sigma_{jj})/2$. Physisorption processes of CO₂/CH₄ were predominantly associated with van der Waals interaction (pairwise dispersion) and electrostatic interaction in molecular simulations. Therefore, a combination of site-site LJ^{41,42} potentials and Columbic potentials was used to calculate the intermolecular interaction (including CH₄-CH₄, CH₄-CO₂ and CO₂-CO₂) and the gas-framework interaction. The site-site LJ potential was described by the LJ (12, 6) model, and the electrostatic interaction was calculated via the Coulomb law.

2.3 Grand canonical Monte Carlo (GCMC) simulations

As shown in Fig. 2, hypothetical edge-functionalized NPCs with periodic boundary conditions were assumed as the simulation boxes.

The NPCs was constructed from a collective of flat coronene-shaped graphitic basis units.¹² The mass density of all edge-functionalized NPCs was kept as 0.542 g/cm³.¹² Five NPCs structures were considered, including (a) NPC, a collective of flat coronene-shaped graphitic basis units; (b) H-NPC, a collective of flat coronene; (c-e) OH-NPC, NH₂-NPC, and COOH-NPC, a collective of basis units with hydroxyl, amino, and carboxyl groups, respectively. The Peng-Robinson equation of state was chosen to calculate the gas-phase density and experimental fugacity.^{43,44} GCMC simulations were performed to estimate the adsorption isotherms and the selectivity consisting of 25 state points at temperatures of 298, 313 and 373 K and at pressures up to 20.00 MPa. For each state point, the configuration number of 4×10^6 was chosen to guarantee the equilibration of the gas-framework system, followed by 6×10^6 configurations sampled to analyze the thermodynamic properties. All the molecular modeling was carried out by an object-oriented multipurpose simulation code (MuSiC).⁴⁵

Benchmark of the computational methodology, including pore topology and morphology, DFT, Mulliken charge analysis, and GCMC simulation are provided in ESI†. The combination of DFT and GCMC was calibrated in detail in our recent investigation.²⁰

3. Results

The adsorption capacity of single-component CO₂/CH₄ in edge-functionalized NPCs is first estimated. Thereafter, the competitive adsorption of binary CO₂/CH₄ mixture is determined by using the selectivity analysis.

3.1 Single-component adsorption of CO₂/CH₄

Fig. 3 shows the absolute adsorption isotherms of the single-component adsorption of CO₂/CH₄, which are modeled independently using the GCMC simulation. The total uptake represents the total molar amount of gas per g (including both condensed and gas phases). Figs. 3a-c show the absolute adsorption isotherms of CO₂ in edge-functionalized NPCs at 298, 313, and 373

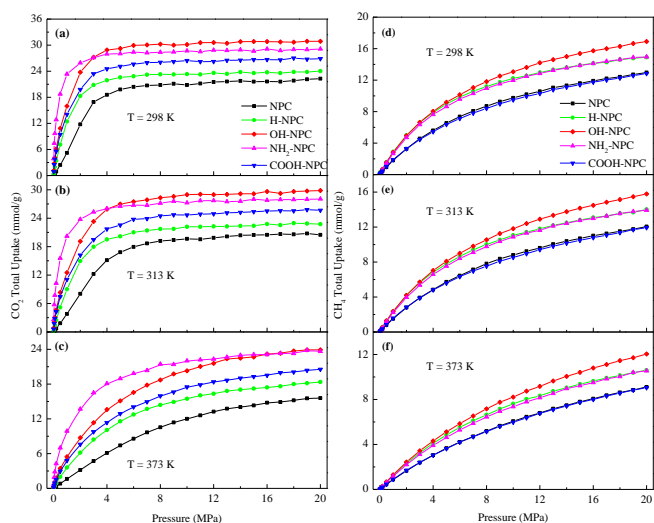


Fig. 3 Absolute adsorption isotherms of CO₂ (a-c) and CH₄ (d-f) in edge-functionalized NPCs.

K, respectively. The total CO₂ uptake in edge-functionalized NPCs is obviously higher than the corresponding value in NPC, which indicates that edge-functionalization can significantly enhance CO₂ adsorption capacity. The total CO₂ uptake follows the sequence of NH₂-NPC > OH-NPC > COOH-NPC > H-NPC > NPC at low pressure (0-5 MPa), and follows the sequence of OH-NPC > NH₂-NPC > COOH-NPC > H-NPC > NPC at relatively high pressure (5-20 MPa). Obvious intersections are observed between the adsorption isotherms of NH₂- and OH-NPCs, and the intersection appears nearby the saturated adsorption pressure of 3, 4, and 16 MPa at 298, 313, and 373 K, respectively. That is, the intersection shifts towards a higher pressure (*i.e.* the increase of saturated adsorption pressure) with the increase of temperature.

Figs. 3d-f illustrate the absolute adsorption isotherms of CH₄ in edge-functionalized NPCs at 298, 313, and 373 K, respectively. With the exception of COOH-NPC, the introduction of functional groups can enhance the CH₄ adsorption capacity at whole pressure in the sequence of OH-NPC > H-NPC > NH₂-NPC > COOH-NPC/NPC. For COOH-NPC, two strong electronegative O atoms slightly weaken the CH₄ adsorption, whereas for the other NPCs, edge-functionalization has little positive effect on the CH₄ absolute adsorption capacity, which is different from the negative effect of surface-functionalization on CH₄ adsorption density and excess adsorption amount.^{1,20}

Fig. 3 shows that the absolute adsorption isotherms of CH₄ and CO₂ exhibit type-I Langmuir adsorption behaviour, which is a typical characteristic of nanoporous materials.⁴⁶ Obviously, the adsorption capacity of CO₂ is significantly larger than that of CH₄. It is thus expected that CO₂ molecule is superior relative to CH₄ to adsorb in all the edge-functionalized NPCs, especially at low pressure (0-5 MPa). For the temperature effect, the gas adsorption capacity decreases along with the increase of temperature as a result of the exothermic nature of the adsorption process. For instance, at pressures above 5 MPa, the total CO₂ uptakes in edge-functionalized NPCs are within the range of 20.4-30.9, 17.9-29.8 and 8.6-23.9 mmol/g at 298, 313, and 373 K, respectively (see Figs. 3a-c),

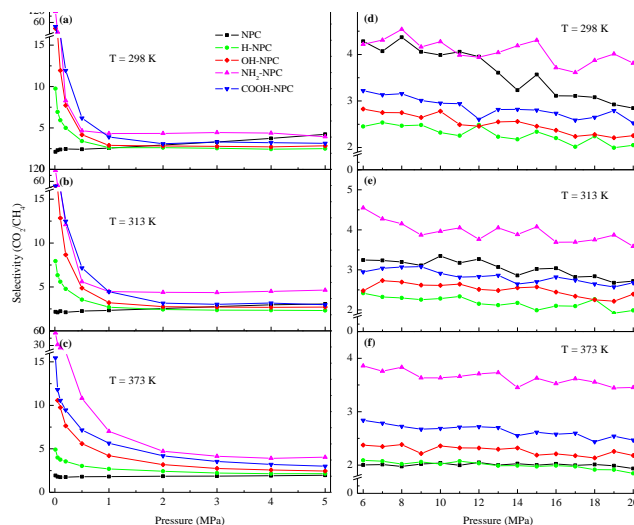


Fig. 4 Selectivity of CO₂ over CH₄ in edge-functionalized NPCs at low (a-c) and high (d-f) pressure.

whereas the total CH₄ uptakes are within the range of 6.5-16.9, 5.7-15.8, and 3.7-12.0 mmol/g under the same conditions (see Figs. 3d-f). Note that the total CO₂ uptake in edge-functionalized NPCs can reach up to ~10.0 mmol/g at 298 K and 0.1 MPa, which is comparable to the current state-of-the-art MOFs (2-12 mmol/g) and greater than other porous carbons (4-8 mmol/g) at similar temperature and pressure.^{47,48}

3.2 Competitive adsorption of binary CO₂/CH₄ mixture

Selectivity is a good indication for porous materials in the capture and separation of certain species from mixed gas systems in CCS process.⁴⁹ The selectivity of CO₂ over CH₄ is defined as follows:

$$S_{\text{CO}_2/\text{CH}_4} = \frac{x_{\text{CO}_2} / x_{\text{CH}_4}}{y_{\text{CO}_2} / y_{\text{CH}_4}} \quad (1)$$

where $S_{\text{CO}_2/\text{CH}_4}$ denotes the selectivity of CO₂ over CH₄, x_{CO_2} and x_{CH_4} are the molar fractions of CO₂ and CH₄ in the adsorbed phase, and y_{CO_2} and y_{CH_4} are the corresponding molar fractions in the bulk gas phase. In the present study, the molar fractions of CO₂ and CH₄ are both kept as 0.5, and thus, selectivity larger than 1.0 indicates that CO₂ preferentially adsorbs over CH₄ throughout the competitive adsorption process.

Fig. 4 shows the adsorption selectivity of CO₂ from an equimolar CO₂/CH₄ mixture in edge-functionalized NPCs at low (0-5 MPa) and high (5-20 MPa) pressures at 298, 313, and 373 K. In Fig. 4, the selectivity of CO₂ over CH₄ in NPC is ~2, which is well consistent with that in the perfect graphite slit pore as reported by Wilcox¹ and that in mesoporous carbon as reported by Lu⁴⁸. The introduction of functional groups significantly increases the selectivity of CO₂ over CH₄, especially at ultra-low pressure. At 0.05 MPa and 298 K, the selectivity of CO₂ over CH₄ increases in the sequence of NPC (~2) < H-NPC (~7) < OH-NPC (~19) < COOH-NPC (~26) < NH₂-NPC (~33) (see Fig. 4a). This enhancement originates mainly from the induced polarity of functional groups, which have a stronger influence on CO₂ with a quadrupole moment than on CH₄ with a

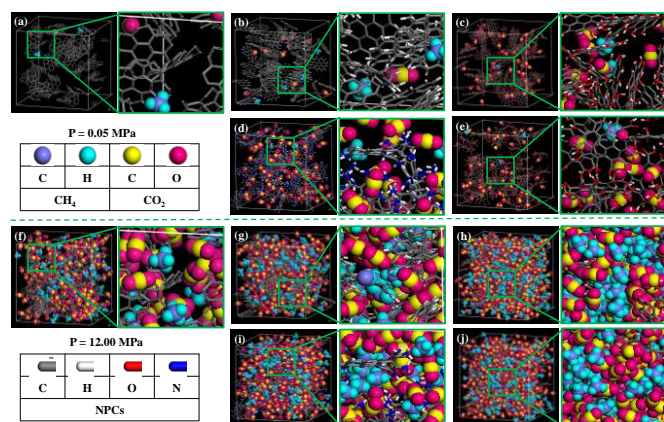


Fig. 5 Snapshots of an equimolar CO_2/CH_4 mixture in NPCs at 298 K and $P = 0.05$ (a-e) and 12.00 (f-j) MPa.

permanent octupole moment.¹ The selectivity in low pressure regions decreases sharply with the increase of pressure, and the trend of selectivity at relatively high pressure shows a small degree of difference with that at low pressure. In addition, the gas adsorption behaviour is sensitive to temperature, and thus, temperature may have a significant influence on the selectivity of CO_2 over CH_4 in edge-functionalized NPCs. Figs. 4d-f indicate that with the increase of temperature, the selectivity of CO_2 over CH_4 in NPC decreases gradually from ~ 4 to ~ 3 and ~ 2 . Moreover, temperature does not affect the selectivity sequence in edge-functionalized NPCs, thus, $\text{NH}_2\text{-NPC} > \text{COOH-NPC} > \text{OH-NPC} > \text{H-NPC}$. This effect may be ascribed to the fact that the electrostatic interaction of gas-framework is independent of temperature. Similar findings about the effects of functional groups in porous carbons were also reported by Wilcox¹ and Lu⁴⁸.

To understand further the distribution of gases adsorbed in edge-functionalized NPCs, the snapshots of equilibrium configurations of binary CO_2/CH_4 mixture at low (0.05 MPa) and high (12 MPa) pressures are provided in Fig. 5. At low pressure, CO_2 molecules adsorb on the pore surface prior to CH_4 molecules. As the pressure increases, CO_2 starts to occupy the pore space, and CH_4 tends to fill the void space left by CO_2 molecules. At high pressure, the

selectivity of CO_2 over CH_4 flattens out to a constant value and keeps a relative balance.

To sum up, edge-functionalization would significantly enhance the single-component adsorption of CO_2/CH_4 , and effectively improve the selectivity of CO_2 over CH_4 , exhibiting potential as an effective and superior alternative strategy in CCS process. The single-component adsorption capacity and selectivity of CO_2 over CH_4 in edge-functionalized NPCs decrease with the increase of temperature. The single-component adsorption capacity increases, while the selectivity of CO_2 over CH_4 decreases with the increase of pressure.

4. Discussion

To provide original insight into the intrinsic essence of edge-functionalization on single-component adsorption and selectivity, the effects on (1) pore topology and morphology, (2) atomic partial charge, (3) adsorption energy, and (4) electrostatic contribution are discussed in this section.

4.1 Pore topology and morphology

Pore topology and morphology play a crucial role in the porosity of gas-accessible framework.⁵⁰ How the functional groups affect pore physical characteristics, such as pore shape, structure, and accessible surface area, is estimated by using the Sarkisov⁵¹ and Duren⁵² methods. These methods evaluate the (1) available pore volume, V_p , (2) pore limiting diameter, D_L , (3) maximum pore diameter, D_M , (4) porosity, Φ , (5) accessible surface area, A .⁵³ Among these variables, V_p is expressed in two terms, namely, available pore volume per unit mass of adsorbent or that in unit cell. Porosity Φ is estimated by V_p/V_{Total} , where V_{Total} is the total volume of the edge-functionalized NPCs unit cell. Physical characterizations of pore topology and morphology are provided in Table 3, and the relevant computational method of V_p is elaborated in ESI†.

Table 3 indicates that OH- and COOH-NPC exhibit relatively large pore spaces of 1.43 and 1.36 cm^3/g and maximum pore diameters of 17.99 and 16.97 Å, respectively. The available pore volume of $\text{NH}_2\text{-NPC}$ (1.35 cm^3/g) is very close to that of COOH-

Table 3 Physical characteristics of the edge-functionalized NPCs

R	None	H-	OH-	$\text{NH}_2\text{-}$	COOH-
Number of basis units (atoms) in unit cell	60 (1440)	60 (2160)	60 (2880)	40 (2400)	40 (2880)
Dimensions (\AA^3)	37.56 ³	38.07 ³	44.89 ³	38.90 ³	46.65 ³
V_p^c ($\times 10^4 \text{\AA}^3/\text{uc}$)	3.47	3.17	6.92	4.17	7.26
V_p^c (cm^3/g)	1.25	1.28	1.43	1.35	1.36
D_L (\AA)	7.06	8.33	11.90	8.19	8.52
D_m (\AA)	12.87	11.26	17.99	12.44	16.97
Porosity, Φ (%)	65.5	57.5	76.5	70.8	71.5
Surface area ^a (m^2/g)	3580	3451	3184	3598	3548
Surface area ^b (m^2/g)	3588	3459	3188	3600	3553
Gas probe molecule $a, b, c = \text{CH}_4, \text{CO}_2$, and He.					

NPC, whereas its maximum pore diameter is close to those of NPC (12.87 Å) and H-NPC (11.26 Å). The available pore volumes for NPC and H-NPC are 1.25 and 1.28 cm³/g, respectively. The porosity of edge-functionalized NPCs ranges from 57.5% to 76.5% (see Table 3), which is slightly smaller than that of COFs.^{54,55} All the pore limiting diameters of edge-functionalized NPCs are ~8.00 Å (see Table 3). Porous carbonaceous materials with a pore size of ~8.00 Å are proven to possess the ability to gain the highest gas adsorption density.⁵⁶⁻⁵⁸ Therefore, these structures may be excellent candidates for CO₂/CH₄ adsorption and separation due to their superior adsorption capacity. The accessible surface area of NPC by CH₄ probe molecule is 3580 m²/g, consistent well with the previous result of ~3610 m²/g.¹² The high degree of agreement of our result with previous finding demonstrates the reliability of our model and levels of theory. The accessible surface area of edge-functionalized NPCs as determined by CH₄ probe molecule ranges from 3184 to 3598 m²/g, which is significantly larger than the BET surface areas of zeolites (260-590 m²/g) and mesoporous silicas (450-1070 m²/g),⁵⁹ within the range of activated and hypothetical high-surface-area carbons (2000-4600 m²/g),⁶⁰ but lower than those of the benzene and representative MOFs and COFs (above 6000 m²/g).⁶⁰ Note that the minimal differences in the surface area are observed using two probe molecules because of the small difference in their kinetic diameters (CH₄, 3.73⁶¹; CO₂, 3.72⁶²), as indicated in Table 3.

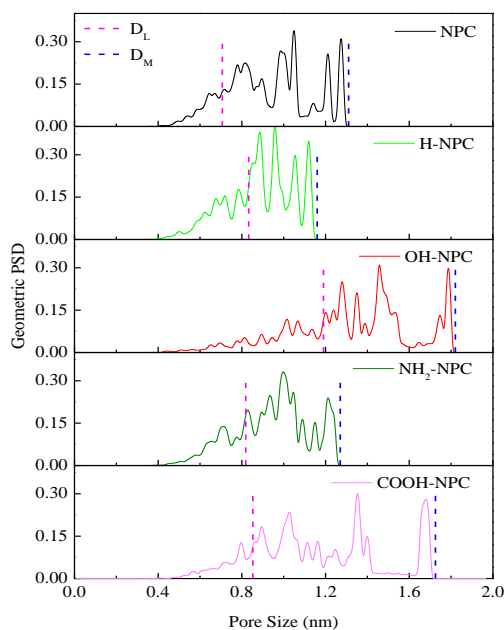


Fig. 6 Geometric PSDs as a function of pore diameter for edge-functionalized NPCs.

To understand further the aforementioned pore structures, pore size distributions (PSDs)⁶³ are analyzed as a function of pore size in Fig. 6. All the PSDs start at a pore size of ~3.52 Å, and contain few small ultramicropores (< 7.00 Å) and large micropores (within 7.00 - 20.00 Å) based on IUPAC classification.⁶⁴ These results agree well with the single-component adsorption isotherms. The PSDs of NPC, H-NPC, and NH₂-NPC, although estimated with different functional

groups, exhibit similar pore shapes and structures. Aside from the similar narrow PSDs, OH- and COOH-NPCs also exhibit an isolated large pore with broad PSDs (see Fig. 6). This result demonstrates that OH- and COOH-NPCs own large pore structures. Particularly, OH-NPC falls within the range of micropore size of (7.50-18.00 Å), exhibiting a fairly dense micropore structure. In addition, the values of D_M and D_L of NPCs are confirmed in Fig. 6.

In summary, the effect of edge-functionalization enhances the effective accessible surface area and enlarges the pore spaces and diameters, especially for the O-containing edge-functionalization NPCs. It therefore creates a favorable environment conducive to gas adsorption for gas-framework systems.

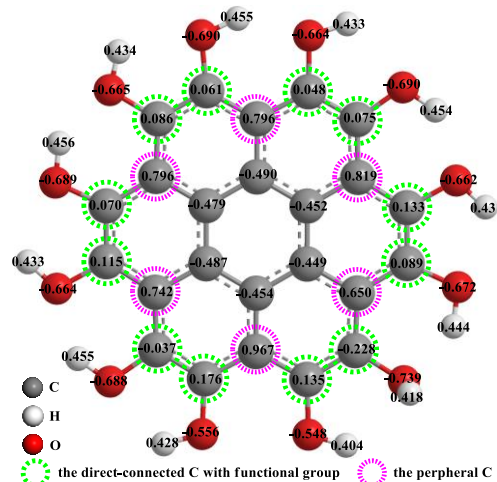


Fig. 7 Atomic partial charges for the OH-basis unit.

4.2 Atomic partial charge

Atomic partial charges are required as input parameters, which would determine the energy contributions in the statistical molecular simulations. Mulliken charge analysis of these edge-functionalized NPCs surfaces are therefore taken into account, as shown in Table 2 and Figs. 7 and S4 (see ESI†). A negative value represents that the relevant atom gains partial electron from the surrounding atoms, therefore exhibiting electronegativity; whereas a positive value indicates the contrary. The distribution of atomic partial charge changes immensely because of the strong potential of accept/donate electrons for the functional groups. As shown in Fig. 7, the O atom in the OH- group exhibits an electronegative potential by accepting electrons of 0.548-0.739 e from the neighboring and peripheral C and H atoms, while the outermost H atoms in functional groups exhibit high electropositivity by donating electrons of 0.404-0.456 e. The inductive effect results in a dramatic electron transfer, and further affects the atomic partial charge of the basal plane.²⁰ Table 2 shows that some C atoms in the basal plane nearly lose an electron and show an ultra-strong electropositivity. Stronger electronegativity of the functional group results in more influence on the atomic partial charge of edge-functionalized basis units. The N and O atoms in the functional groups exhibit strong electronegativity by gaining extra electron densities, especially for N atoms, whereas C and H in the functional groups exhibit opposite effects.

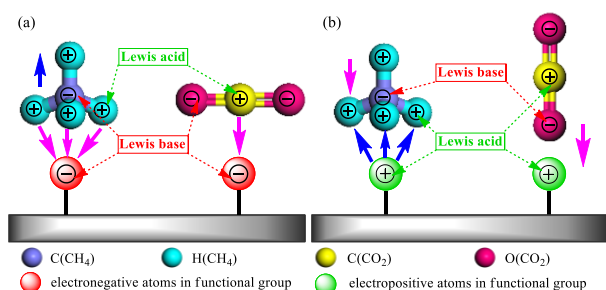


Fig. 8 Schematic display of the interaction between gas molecules and charged atoms in the functional group or basal plane.

Wilcox *et al.*^{1,21,22} have pointed out that an electronegative atom has an increased potential to donate an electron to the proximal adsorbate molecule in the pore space. The O-containing functional group enables strong electron donation, and the transport process depends on the acid-base^{65,66} nature of the adsorbate molecule. Fig. 8 illustrates the interaction between the gas molecule and the charged atoms. As shown in Fig. 8a, the electronegative O and N atoms in functional groups serve as basic adsorption sites on the basal plane, and function as Lewis bases by donating their electron to the acidic C atom of the CO₂ molecule. Therefore, the C atom is attracted and rotates parallel to the functional groups, and the strong Lewis basicity in O- and N-containing functional groups significantly enhances the CO₂ adsorption in edge-functionalized NPCs. On the contrary, the CH₄ molecule is a regular tetrahedron molecule, and the central C atom exhibits high electronegativity because it is surrounded by four electropositive H atoms. The electronegative N and O atoms donating their electron to the acidic H atoms of CH₄ would result in a minor enhancement of CH₄ adsorption. However, a strong repulsive force is also observed between the C atom in CH₄ molecule and the electronegative atoms in the functional groups, thereby offsetting the enhancement of CH₄ adsorption. The electropositive H and C atoms in the functional groups that act as Lewis acids also have a significant influence on gas adsorption, as shown in Fig. 8b. One of the O atoms in the CO₂ molecule is attracted and rotates perpendicular to the functional groups, therefore leading to CO₂ adsorption enhancement. For the CH₄ molecule, the electropositive H atom in the functional groups repels the electropositive H atom, but attracts the C atom in CH₄. More importantly, surface C atoms on the basis unit would serve as basic adsorption sites because of the strong inductive effect caused by the functional groups and act similar roles in gas adsorption behavior, as indicated in the cases of the functional groups.

Overall, the introduction of functional groups enhances CO₂ adsorption by changing the packing pattern of the adsorbed linear CO₂ molecule, whereas CH₄ adsorption relies on the competition between the attractive and repulsive interactions.

4.3 Adsorption energy

To understand the interaction between CO₂/CH₄ and the edge-functionalized NPCs surface, the adsorption energy, E_{ads} , is obtained by equation (2):

$$E_{ads} = E_{adsorbate} + E_{surf} - E_{adsorbate+surf} \quad (2)$$

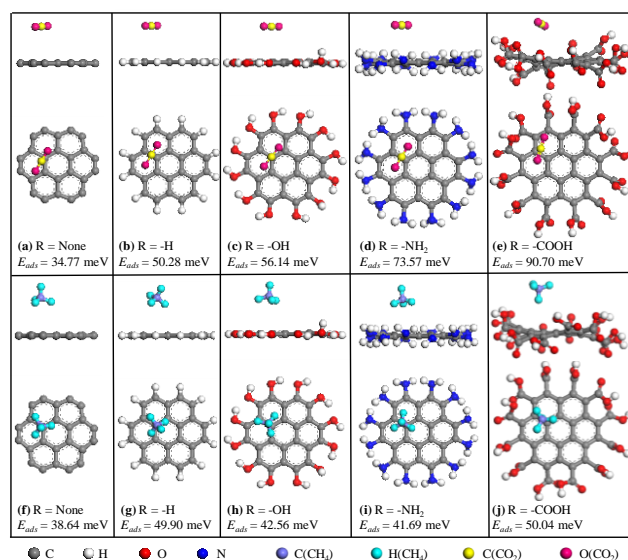


Fig. 9 Stable adsorption configurations (side view (up) and top view (down)) of CO₂ (a-e) and CH₄ (f-j) on edge-functionalized basis unit at the B1 site.

where $E_{adsorbate}$ is the energy of the gas species, E_{surf} is the energy of the edge-functionalized NPC surface, and $E_{adsorbate+surf}$ is the total energy of the gas molecule adsorbed on edge-functionalized NPC surface. Based on the definition, a larger positive value implies more stable adsorption. CO₂/CH₄ molecules can approach the edge-functionalized NPC surface in every direction (T, B, and H). However, exploring all possible stable adsorption structures is a tremendous and unfeasible task. Herein, specific directions are selected by optimizing a single CO₂/CH₄ molecule adsorbed on coronene, as illustrated in Figs. S5 and S6 (see ESI†). Noted that adsorption energies and configurations may provide a basic insight into the adsorbate-adsorbent interaction, like that in Jiang's work.⁶⁷

The B direction possesses the largest number of stable sites for CH₄/CO₂ adsorption, therefore, B1 is chosen first to investigate the effect of edge-functionalization on adsorption energy, as shown in Fig. 9. Results show that the introduction of functional groups has a significant influence, through the inductive effect, on the gas adsorption on the basis unit surface. For the basis unit, the adsorption energy of CO₂ is 34.77 meV, which is slightly lower than 38.64 meV for CH₄. This difference indicates that the surface site is energetically favorable for CH₄ with respect to CO₂, similar to CO₂/CH₄ adsorbed in the (10, 0) and (5, 5) single-walled carbon nanotube (SWNT).⁶⁸ While the basis unit is saturated with H, namely, coronene, the adsorption energy for both gas molecules is enhanced by at least 29%, reaching 50.28 meV for CO₂ and 49.90 meV for CH₄. The OH- group increases the adsorption energy of CO₂ to 56.14 meV and weakens that of CH₄ to 42.56 meV. When comparing the adsorption energy for the OH-basis unit with that of the basis unit, the enhancement percentages of CO₂ and CH₄ are 61.46% and 10.14%, respectively. Therefore, the embedding of the OH- group could effectively increase the discrimination between CO₂ and CH₄ adsorption. This contribution is clearly from the cooperative effect of electronegative O atoms and electropositive H

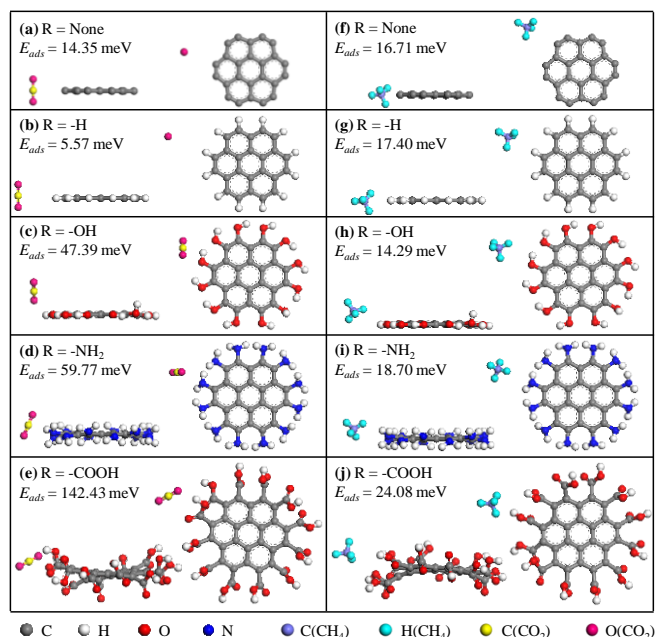


Fig. 10 Stable adsorption configurations (side view (up) and top view (down)) of CO₂ (a-e) and CH₄ (f-j) on edge-functionalized basis unit from the initial S direction.

atoms, as shown in Fig. 8. The introduction of the NH₂– group improves the adsorption energy of CO₂ up to 73.57 meV, but only has a slight influence on the adsorption energy of CH₄ to 41.69 meV. Compared with the OH– basis unit, two strong electronegative O atoms in the COOH– group further boost this trend, therefore increasing the adsorption energy of CO₂ on COOH– basis unit to as high as 90.70 meV and that of CH₄ to 54.04 meV.

Along the S direction, the adsorption energy is directly affected by the electrostatic interaction when the gas molecule approaches the functional group, as shown in Fig. 10. Similar to the cases at the B1 site, the adsorption energy of CH₄ at the S site is 16.71 meV, slightly larger than 14.35 meV for CO₂ on the basis unit. For coronene, the emergence of electropositive H atoms in functional groups decreases the adsorption stability of CO₂ to 5.57 meV and slightly increases the adsorption energy of CH₄ to 17.40 meV. Compared with the H– group, the OH– group significantly enhances the adsorption energy of CO₂ to 47.39 meV, and slightly decreases the value of CH₄ to 14.29 meV. From another point of view, the O atom in the OH– group significantly increases the CO₂ adsorption energy by 750.81%, and slightly decreases that of CH₄ by 17.87% relative to the corresponding value on the coronene. For the COOH– group, the emergence of two strong electronegative O atoms in a functional group further increases the adsorption energy of CO₂ up to 142.43 meV, but slightly increases that of CH₄ to 24.08 meV. Hence, stronger group's electronegativity indicates more stable adsorption for CO₂ at the S site. The electronegativity of the NH₂– group falls between those of the OH– and COOH– groups, correspondingly, the adsorption energy of CO₂ (59.77 meV) and CH₄ (18.70 meV) also fall between them.

In summary, the introduction of functional groups has a more positive influence on CO₂ than on CH₄ for surface/edge adsorption

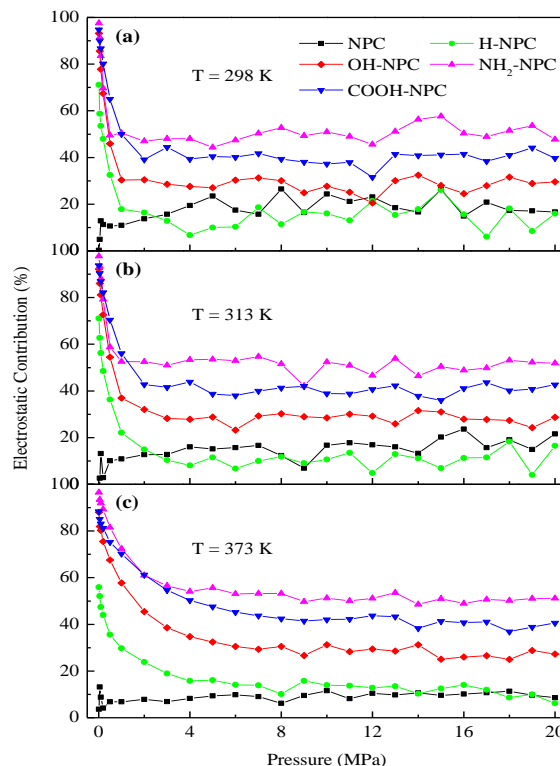


Fig. 11 Electrostatic contribution of edge-functionalized NPCs with atomic partial charge on the selectivity of CO₂ over CH₄.

enhancement through inductive effect/direct interaction. Combined with atomic charge analysis, stronger electronegativity leads to more stable adsorption for CO₂, but has a slight influence on surface/edge adsorption for CH₄. Therefore, the stronger electronegative group embedded in edge-functionalized NPCs would lead to the higher competitive adsorption advantage of CO₂ in CO₂/CH₄ mixture.

4.4 Electrostatic contribution

To grasp the effect of electrostatic interaction on the adsorption selectivity of CO₂ over CH₄, GCMC simulations with or without electrostatic interaction of gas-framework are performed. The corresponding absolute adsorption isotherms of CO₂/CH₄ in edge-functionalized NPCs with or without electrostatic interaction are presented in Figs. S7 and S8 (see ESI†), respectively. The electrostatic contribution can be evaluated by applying equation (3):⁶⁹

$$\text{Electrostatic contribution} = \frac{S_{\text{with}} - S_{\text{without}}}{S_{\text{with}}} \times 100\% \quad (3)$$

where $S_{\text{with}}/S_{\text{without}}$ is the selectivity with or without the gas-framework electrostatic interaction. Fig. 11 shows the electrostatic contribution of gas-framework on the selectivity of CO₂ over CH₄ at three temperatures. Edge-functionalized NPCs clearly show an extraordinarily large electrostatic contribution at low pressure, reaching even up to 98% at the ultralow pressure level, which indicates that electrostatic interaction plays a more significant role in the selectivity at low pressure than at high pressure. Subsequently, electrostatic contribution decreases with the increase of pressure, until reaching a constant value after ~5 MPa. The results are easy to

understand by analyzing the filling process. The gas molecules first occupy the region close to the pore surface due to the strong electrostatic interaction at low pressure. In this process, the functional groups exhibit stronger electrostatic interaction because of their higher accepting/donating electron densities, and therefore, enhance the total CO₂ uptake. With the increase of pressure, the gas molecules are gradually filled in the whole pore space, and the gas-gas interaction becomes stronger and stronger, thereby increasing the influence from PSDs at high pressure. In general, larger pore spaces with higher atomic partial charge show larger gas total uptakes, as with NH₂- and OH-NPCs. These results originate from the synergetic effects of PSDs and electrostatic interaction.

Atomic partial charge has a great effect on the electrostatic contribution and the selectivity of CO₂ over CH₄. The higher atomic partial charge in the specific functional group leads to the stronger electronegativity/electropositivity, and generates a larger electrostatic contribution on the selectivity of CO₂ over CH₄. At equilibrium level, the electrostatic contribution of gas-framework systems follows the sequence of NH₂-NPC (~50%) > COOH-NPC (~42%) > OH-NPC (~30%) > H-NPC/NPC (~12%) (see Fig. 11). This result is well consistent with the analyses of the atomic partial charge and adsorption energy: (1) The NH₂- group with the highest atomic partial charge has the largest electrostatic contribution; (2) the electrostatic contribution of the COOH- group with two electronegative O atoms is obviously larger than that of the OH- group with a single electronegative O atom; (3) the OH- group has a larger electrostatic contribution than the H- group because of the existence of a strong electronegative O atom; (4) the electropositive H atom in functional groups has a positive effect on the selectivity of CO₂ over CH₄, and therefore, H-NPC exhibits a slightly larger electrostatic contribution relative to NPC; and (5) NPC with only a small atomic partial charges has little influence on the electrostatic contribution, and thus the selectivity is kept almost as a constant value in the whole pressure region. In addition, temperature has no obvious influence on the electrostatic contribution considering that electrostatic interaction is independent of temperature.

These results clearly support that edge-functionalization may be an effective and superior alternative strategy to enhance CO₂ adsorption and separation performance in CCS process. Edge-functionalized NPCs are comparable to the most effective strategy of doping metal ions, such as Li-modified MOFs (~80%),⁴⁸ in enhancing the gas-framework interaction and selectivity.

5. Conclusions

The effects of edge-functionalization on the competitive adsorption of binary CO₂/CH₄ mixture in NPCs have been systematically investigated by combining DFT and GCMC simulation. The main points are summarized as follows:

(1) Edge-functionalization significantly enhances CO₂ adsorption but has a less influence on CH₄ adsorption for single-component CO₂/CH₄ adsorption, and therefore significantly improving the selectivity of CO₂ over CH₄, in the sequence of NH₂-NPC > COOH-NPC > OH-NPC > H-NPC > NPC at low pressure.

(2) Edge-functionalization creates a conducive environment with large pore size and effective accessible surface area. Higher atomic

partial charge in the functional groups leads to stronger electronegativity/electropositivity, which generates a larger electrostatic contribution on the selectivity of CO₂ over CH₄. The N and O atoms in the functional group exhibit strong electronegativity by gaining electron densities, whereas the C and H atoms in the functional group show the opposite effect.

(3) The edge-functionalized NPCs are energetically favorable for CO₂ adsorption due to the strong electronegative atoms changing the packing pattern of the adsorbed linear CO₂ molecules, but have less effect on CH₄ adsorption because of the competition between the attractive and repulsive interactions through the inductive effect/direct interaction on surface/edge adsorption.

(4) Temperature has a negative influence on the gas adsorption because of the exothermic nature of the adsorption process, but has no obvious influence on the electrostatic contribution on selectivity. With the increase of pressure, the selectivity of CO₂ over CH₄ first decreases sharply and subsequently flattens out to a constant value, corresponding to the influence of electrostatic contribution on selectivity.

This work not only highlights the potential of edge-functionalized NPCs as excellent candidates for the competitive adsorption, capture, and separation for binary CO₂/CH₄ mixture, but also provides an effective and superior alternative strategy in the design and screening of adsorbent materials for CCS application.

Acknowledgements

This work was supported by NSFC (21303266), Shandong Province Natural Science Foundation (ZR2011EMZ002), Promotive Research Fund for Excellent Young and Middle-aged Scientists of Shandong Province (BS2013CL031), PetroChina Innovation Foundation (2013D-5006-0406), and the Fundamental Research Funds for the Central Universities (13CX05020A and 13CX02025A). We also thank Key Laboratory of Artificial Structures and Quantum Control for the supporting.

Notes and References

1. Y. Y. Liu and J. Wilcox, *Environ. Sci. Technol.*, 2012, **47**, 95-101.
2. C. M. White, D. H. Smith, K. L. Jones, A. L. Goodman, S. A. Jikich, R. B. LaCount, S. B. DuBose, E. Ozdemir, B. I. Morsi and K. T. Schroeder, *Energy Fuels*, 2005, **19**, 659-724.
3. M. Mazzotti, R. Pini and G. Storti, *J. Supercrit. Fluid.*, 2009, **47**, 619-627.
4. D. F. Zhang, S. G. Li, Y. J. Cui, W. L. Song and W. G. Lin, *Ind. Eng. Chem. Res.*, 2011, **50**, 8742-8749.
5. B. Wang, A. P. Cote, H. Furukawa, M. O'Keeffe and O. M. Yaghi, *Nature*, 2008, **453**, 207-211.
6. H. Furukawa, N. Ko, Y. B. Go, N. Aratani, S. B. Choi, E. Choi, A. Ö. Yazaydin, R. Q. Snurr, M. O'Keeffe, J. Kim and O. M. Yaghi, *Science*, 2010, **329**, 424-428.
7. M. X. Shan, Q. Z. Xue, N. N. Jing, C. C. Ling, T. Zhang, Z. F. Yan and J. T. Zheng, *Nanoscale*, 2012, **4**, 5477-5482.
8. Y. Kurniawan, S. K. Bhatia and V. Rudolph, *AIChE J.*, 2006, **52**, 957-967.

9. S. Furmaniak, P. Kowalczyk, A. P. Terzyk, P. A. Gauden and P. J. Harris, *J. Colloid Interf. Sci.*, 2013, **397**, 144-153.
10. P. Billemont, B. Coasne and G. De Weireld, *Langmuir*, 2013, **29**, 3328-3338.
11. P. Billemont, B. Coasne and G. De Weireld, *Adsorption*, 2014, **20**, 453-463.
12. K. V. Kumar, E. A. Müller and F. Rodríguez-Reinoso, *J. Phys. Chem. C*, 2012, **116**, 11820-11829.
13. J. C. Palmer, J. D. Moore, T. J. Roussel, J. K. Brennan and K. E. Gubbins, *Phys. Chem. Chem. Phys.*, 2011, **13**, 3985-3996.
14. Y. Jiao, A. Du, M. Hankel and S. C. Smith, *Phys. Chem. Chem. Phys.*, 2013, **15**, 4832-4843.
15. S. K. Jain, J. P. Pikunic, R. J.-M. Pellenq and K. E. Gubbins, *Adsorption*, 2005, **11**, 355-360.
16. S. K. Jain, R. J.-M. Pellenq, J. P. Pikunic and K. E. Gubbins, *Langmuir*, 2006, **22**, 9942-9948.
17. S. K. Jain, K. E. Gubbins, R. J.-M. Pellenq and J. P. Pikunic, *Carbon*, 2006, **44**, 2445-2451.
18. L. Brochard, M. Vandamme, R. J.-M. Pellenq and T. Fen-Chong, *Langmuir*, 2012, **28**, 2659-2670.
19. C. M. Tenney and C. M. Lastoskie, *Environ. Prog.*, 2006, **25**, 343-354.
20. D. L. Jin, X. Q. Lu, M. M. Zhang, S. X. Wei, Q. Zhu, X. F. Shi, Y. Shao, W. L. Wang and W. Y. Guo, *Phys. Chem. Chem. Phys.*, 2014, **16**, 11037-11046.
21. Y. Y. Liu and J. Wilcox, *Environ. Sci. Technol.*, 2012, **46**, 1940-1947.
22. Y. Y. Liu and J. Wilcox, *Int. J. Coal Geol.*, 2012, **104**, 83-95.
23. V. S. Kandagal, A. Pathak, K. G. Ayappa and S. N. Punathanam, *J. Phys. Chem. C*, 2012, **116**, 23394-23403.
24. M. J. Frisch, G. W. Trucks, H. B. Schlegel, G. E. Scuseria, M. A. Robb, J. R. Cheeseman, G. Scalmani, V. Barone, B. Mennucci, G. A. Petersson, H. Nakatsuji, M. Caricato, X. Li, H. P. Hratchian, A. F. Izmaylov, J. Bloino, G. Zheng, J. L. Sonnenberg, M. Hada, M. Ehara, K. Toyota, R. Fukuda, J. Hasegawa, M. Ishida, T. Nakajima, Y. Honda, O. Kitao, H. Nakai, T. Vreven, J. A. Montgomery, Jr, J. E. Peralta, F. Ogliaro, M. Bearpark, J. J. Heyd, E. Brothers, K. N. Kudin, V. N. Staroverov, R. Kobayashi, J. Normand, K. Raghavachari, A. Rendell, J. C. Burant, S. S. Iyengar, J. Tomasi, M. Cossi, N. Rega, J. M. Millam, M. Klene, J. E. Knox, J. B. Cross, V. Bakken, C. Adamo, J. Jaramillo, R. Gomperts, R. E. Stratmann, O. Yazyev, A. J. Austin, R. Cammi, C. Pomelli, J. W. Ochterski, R. L. Martin, K. Morokuma, V. G. Zakrzewski, G. A. Voth, P. Salvador, J. J. Dannenberg, S. Dapprich, A. D. Daniels, O. Farkas, J. B. Foresman, J. V. Ortiz, J. Cioslowski and D. J. Fox, *GAUSSIAN 09 (Revision A.01)*, Gaussian, Inc., Wallingford, CT, 2009, **270**, 271.
25. B. S. Jursic, *J. Mol. Struct.: THEOCHEM*, 1998, **452**, 145-152.
26. S. C. Xu, S. Irle, D. G. Musaev and M. C. Lin, *J. Phys. Chem. C*, 2009, **113**, 18772-18777.
27. L. R. Radovic, *J. Am. Chem. Soc.*, 2009, **131**, 17166-17175.
28. S. Tsuzuki, K. Honda, T. Uchimaru, M. Mikami and K. Tanabe, *J. Am. Chem. Soc.*, 2000, **122**, 3746-3753.
29. B. Delley, *J. Chem. Phys.*, 2000, **113**, 7756-7764.
30. B. Delley, *J. Phys. Chem.*, 1996, **100**, 6107-6110.
31. J. P. Perdew, K. Burke and M. Ernzerhof, *Phys. Rev. Lett.*, 1996, **77**, 3865-3868.
32. D.-H. Lim, A. S. Negreia and J. Wilcox, *J. Phys. Chem. C*, 2011, **115**, 8961-8970.
33. Z. M. Ao, S. Li and Q. Jiang, *Solid State Commun.*, 2010, **150**, 680-683.
34. B. Delley, *Phys. Rev. B*, 2002, **66**, 155125-155134.
35. J. J. Potoff and J. I. Siepmann, *AIChE J.*, 2001, **47**, 1676-1682.
36. Y. X. Sun, D. Spellmeyer, D. A. Pearlman and P. Kollman, *J. Am. Chem. Soc.*, 1992, **114**, 6798-6801.
37. A. K. Rappé, C. J. Casewit, K. S. Colwell, W. A. Goddard III and W. M. Skiff, *J. Am. Chem. Soc.*, 1992, **114**, 10024-10035.
38. A. K. Rappe, K. S. Colwell and C. J. Casewit, *Inorg. Chem.*, 1993, **32**, 3438-3450.
39. C. J. Casewit, K. S. Colwell and A. K. Rappe, *J. Am. Chem. Soc.*, 1992, **114**, 10035-10046.
40. C. J. Casewit, K. S. Colwell and A. K. Rappe, *J. Am. Chem. Soc.*, 1992, **114**, 10046-10053.
41. A. M. Tsvelik and A. Macdonald, *Phys. Today*, 1997, **50**, 66.
42. A. A. Clifford, P. Gray and N. Platts, *J. Chem. Soc., Faraday Trans. 1*, 1977, **73**, 381-382.
43. D.-Y. Peng and D. B. Robinson, *Ind. Eng. Chem. Fundamen.*, 1976, **15**, 59-64.
44. R. C. Reid, J. M. Prausnitz and B. E. Poling, *The properties of gases and liquids*, New York: McGraw-Hill, 1987.
45. A. Gupta, S. Chempath, M. J. Sanborn, L. A. Clark and R. Q. Snurr, *Mol. Simulat.*, 2003, **29**, 29-46.
46. S. Brunauer, L. S. Deming, W. E. Deming and E. Teller, *J. Am. Chem. Soc.*, 1940, **62**, 1723-1732.
47. D. M. D'Alessandro, B. Smit and J. R. Long, *Angew. Chem. Int. Ed.*, 2010, **49**, 6058-6082.
48. L. H. Lu, S. S. Wang, E. A. Müller, W. Cao, Y. D. Zhu, X. H. Lu, G. Jackson, *Fluid Phase Equilibria*, 2014, **362**, 227-234.
49. Y. H. Liu, D. H. Liu, Q. Y. Yang, C. L. Zhong and J. G. Mi, *Ind. Eng. Chem. Res.*, 2010, **49**, 2902-2906.
50. K. Konstas, T. Osl, Y. X. Yang, M. Batten, N. Burke, A. J. Hill and M. R. Hill, *J. Mater. Chem.*, 2012, **22**, 16698-16708.
51. L. Sarkisov and A. Harrison, *Mol. Simulat.*, 2011, **37**, 1248-1257.
52. T. Düren, F. Millange, G. Férey, K. S. Walton and R. Q. Snurr, *J. Phys. Chem. C*, 2007, **111**, 15350-15356.
53. H. Frost, T. Düren and R. Q. Snurr, *J. Phys. Chem. B*, 2006, **110**, 9565-9570.
54. H. Furukawa and O. M. Yaghi, *J. Am. Chem. Soc.*, 2009, **131**, 8875-8883.
55. Z. H. Xiang and D. P. Cao, *J. Mater. Chem. A*, 2013, **1**, 2691-2718.
56. X. S. Chen, B. McEnaney, T. J. Mays, J. Alcaniz-Monge, D. Cazorla-Amoros and A. Linares-Solano, *Carbon*, 1997, **35**, 1251-1258.
57. K. A. Sosin and D. F. Quinn, *J. Porous Mater.*, 1995, **1**, 111-119.
58. L. Huang, Z. H. Xiang and D. P. Cao, *J. Mater. Chem. A*, 2013, **1**, 3851.
59. G. Garberoglio, *Langmuir*, 2007, **23**, 12154-12158.
60. B. Kuchta, L. Firlej, A. Mohammadhosseini, P. Boulet, M. Beckner, J. Romanos and P. Pfeifer, *J. Am. Chem. Soc.*, 2012, **134**, 15130-15137.
61. M. G. Martin and J. I. Siepmann, *J. Phys. Chem. B*, 1998, **102**, 2569-2577.
62. J. Zhou and W. C. Wang, *Langmuir*, 2000, **16**, 8063-8070.
63. L. D. Gelb and K. E. Gubbins, *Langmuir*, 1999, **15**, 305-308.
64. K. S. W. Sing, D. H. Everett, R. A. W. Haul, L. Moscou, R. A. Pierotti, J. Rouquerol and T. Siemieniewska, *Pure Appl. Chem.*, 1985, **57**, 603-619.
65. W. B. Jensen, *The Lewis acid-base concepts: an overview*, New York: Wiley, 1980.

66. H. Yamamoto, *Lewis acid reagents: a practical approach*, Oxford University Press, 1999.
67. J. W. Jiang and S. I. Sandler, *J. Am. Chem. Soc.*, 2005, **127**, 11989-11997.
68. J. J. Zhao, A. Buldum, J. Han and J. P. Lu, *Nanotechnology*, 2002, **13**, 195-200.
69. Q. Xu, D. H. Liu, Q. Y. Yang, C. L. Zhong and J. Q. Mi, *J. Mater. Chem.*, 2010, **20**, 706-714.